Research Square

Preprints are preliminary reports that have not undergone peer review.
They should not be considered conclusive, used to inform clinical practice,
or referenced by the media as validated information.

INSR as a Potential Target of Bisphenol F-Induced Type 2 Diabetes: Causal Inference and Mechanistic Elucidation via Mendelian Randomization, Multi-Omics Integration, Single-Cell Transcriptomics, and Molecular Docking

Yunpeng You[1]
First Affiliated Hospital of Nanchang University
Yidan Fan[1]
First Affiliated Hospital of Nanchang University
Zhenzhong Zhang[1]
First Affiliated Hospital of Nanchang University
Wengang Deng[1]
First Affiliated Hospital of Nanchang University
Shipeng Huang[1]
First Affiliated Hospital of Nanchang University
Jian Tao[1]
ndyfy06659@ncu.edu.cn

First Affiliated Hospital of Nanchang University

Article

Keywords: Bisphenol F, Type 2 diabetes, INSR, Mendelian randomization, Single-cell sequencing, Machine learning

Posted Date: March 25th, 2026

DOI: https://doi.org/10.21203/rs.3.rs-9201479/v1

License: This work is licensed under a Creative Commons Attribution 4.0 International License.
Read Full License

Additional Declarations: No competing interests reported.

INSR as a Potential Target of Bisphenol F-Induced Type 2 Diabetes: Causal Inference and Mechanistic Elucidation via Mendelian Randomization, Multi-Omics Integration, Single-Cell Transcriptomics, and Molecular Docking

Yunpeng You[1], Yidan Fan[1], Zhenzhong Zhang[1], Wengang Deng[1], Shipeng Huang[1], Jian Tao[1]*

Affiliations

[1]Department of Emergency Medicine, the First Affiliated Hospital of Nanchang University, Nanchang 330006, Jiangxi, China.

Correspondence to: Jian Tao (email: ndyfy06659@ncu.edu.cn)

Abstract

Background: Bisphenol F (BPF), a widely adopted substitute for bisphenol A, is a suspected endocrine-disrupting chemical; however, its causal relationship with type 2 diabetes mellitus (T2D) and the underlying molecular mechanisms remain inadequately characterized.

Methods: Two-sample Mendelian randomization (MR) using European GWAS data evaluated the causal effect of BPF exposure on T2D and eight common diabetic complications. Differential expression analysis and weighted gene co-expression network analysis (WGCNA) were applied to GSE76894 to identify T2D-associated genes. Three machine learning algorithms—Random Forest, XGBoost, and LASSO regression—were integrated to identify the core gene, with diagnostic performance

validated in GSE64998. Single-cell RNA sequencing data (GSE255566) were analyzed using Seurat for immune cell annotation and CellChat for intercellular communication profiling. Molecular docking and 100 ns molecular dynamics (MD) simulation were conducted to characterize BPF–INSR interaction.

Results: MR analysis demonstrated a significant positive causal association between BPF exposure and T2D (OR = 1.006, 95% CI: 1.000–1.013, P = 0.040), with sensitivity analyses confirming robustness. All three machine learning algorithms converged on INSR (insulin receptor) as the sole core gene; INSR was significantly upregulated in T2D and achieved an AUC of 0.92 in the training set and 0.82 in the independent validation set. ScRNA-seq analysis identified five peripheral blood immune cell types, revealing a marked reduction in neutrophil proportion alongside monocyte expansion in T2D; INSR exhibited the highest expression in monocytes. CellChat analysis identified the IGF1–INSR ligand–receptor pair as a central intercellular communication axis, with monocytes functioning as the primary signaling hub and monocyte–neutrophil communication showing the strongest interaction intensity. Molecular docking confirmed stable BPF binding within the INSR ligand-binding pocket ($\Delta G = -6.7$ kcal/mol) at key residues Tyr232, Met56, and Ala227, with MD simulation corroborating complex stability over 100 ns.

Conclusion: This integrative multi-omics study establishes a genetic causal link between BPF exposure and T2D and identifies INSR as the core molecular target mediating BPF-induced metabolic and immune dysregulation, providing a

mechanistic framework and a candidate biomarker for environmentally driven insulin resistance.

Keywords: Bisphenol F; Type 2 diabetes; INSR; Mendelian randomization; Single-cell sequencing; Machine learning

1 Introduction

Type 2 diabetes mellitus (T2D) represents a major global public health challenge with a continuously rising incidence driven by lifestyle changes and population aging. According to the International Diabetes Federation (IDF), approximately 537 million adults currently live with diabetes worldwide—more than 90% of whom have T2D—and this figure is projected to reach 783 million by 2045 [1]. T2D and its associated complications, including cardiovascular disease, nephropathy, neuropathy, and retinopathy, impose a severe burden on both patients' quality of life and global healthcare systems[2, 3]. Despite considerable advances in glucose-lowering therapies, the complex molecular networks underlying the interplay between environmental exposures and genetic susceptibility in T2D pathogenesis remain incompletely understood [4], underscoring the urgent need to identify key driver genes and their regulatory mechanisms to facilitate precision prevention and treatment.

Bisphenol F (BPF), an emerging structural analogue and substitute for bisphenol A (BPA), is widely present in food packaging, receipt paper, and resin-based consumer products. Epidemiological evidence has linked urinary BPF levels to increased insulin resistance, elevated fasting glucose, and higher T2D risk [5].

Mechanistically, BPF may disrupt metabolic homeostasis by interfering with nuclear receptor signaling (e.g., estrogen and androgen receptors), impairing pancreatic β-cell function and insulin secretion, and inducing oxidative stress and chronic inflammation. Additionally, BPF may persistently remodel metabolism-related gene expression profiles through epigenetic modifications such as DNA methylation and histone modification [6]. Nevertheless, the causal relationship between BPF exposure and T2D has not been definitively established, and its key molecular targets, transcriptomic impact, and potential as a diagnostic biomarker or therapeutic target remain to be systematically elucidated.

Immune microenvironment dysregulation is increasingly recognized as a central feature of T2D pathogenesis[7]. Peripheral blood and tissue-infiltrating immune cells—including monocytes/macrophages, T cells, B cells, and neutrophils—form complex intercellular communication networks that collectively drive insulin resistance and β-cell dysfunction through the coordinated secretion of inflammatory mediators[8]. Notably, growing evidence suggests that environmental endocrine disruptors such as BPF may exacerbate this immunometabolic imbalance by modulating immune cell recruitment, polarization, and functional states, thereby promoting a pro-inflammatory metabolic microenvironment[9, 10]. Systematic characterization of immune cell heterogeneity and dynamic intercellular interactions in T2D therefore holds significant value for uncovering disease mechanisms and informing novel immunomodulatory therapeutic strategies.

The rapid advancement of high-throughput sequencing and computational biology has rendered integrated multi-omics analysis a powerful approach for dissecting complex disease mechanisms. Bulk RNA sequencing (bulk RNA-seq) provides comprehensive gene expression profiles at the tissue or cell-population level [11], while single-cell RNA sequencing (scRNA-seq) further resolves cellular heterogeneity, identifies novel functional cell subsets, and enables systematic mapping of intercellular communication networks at single-cell resolution [12]. When combined with Mendelian randomization (MR) for causal inference, network toxicology for target prediction, and machine learning for biomarker discovery, these technologies constitute a rigorous analytical framework for tracing the molecular consequences of environmental exposures through to disease phenotypes.

Building on this background, the present study aimed to systematically investigate the potential molecular mechanisms linking BPF exposure to T2D using an integrative multi-omics and computational approach. MR analysis based on large-scale European GWAS datasets was performed to explore the potential causal relationship between BPF exposure and T2D and its related complications. Network toxicology, differential expression analysis, and weighted gene co-expression network analysis (WGCNA) were integrated to identify candidate genes associated with BPF-related T2D. Machine learning algorithms, including Random Forest, XGBoost, and LASSO regression, were applied to prioritize key genes. In addition, gene set enrichment analysis (GSEA) and scRNA-seq were used to characterize functional pathways and cellular distribution, while molecular docking and molecular dynamics

simulations were conducted to evaluate potential interactions between BPF and target proteins.

2 Materials and Methods

2.1 Data Acquisition and Preprocessing

Genome-wide association study (GWAS) summary statistics for T2D, DM_RETINOPATHY_EXMORE, DM_NEUROPATHY, DM_NEPHROPATHY_EXMORE, DM_MACULOPATHY_EXMORE, DM_KETOACIDOSIS, DM_HYPOGLYC, and E4_DM2PERIPH were retrieved from the FinnGen database (https://www.finngen.fi/) (Table S1). BPF exposure-associated genetic variant data were sourced from the GWAS Catalog database (https://www.ebi.ac.uk/gwas/home). SNPs reaching genome-wide significance for BPF exposure ($P < 5\times10^{-6}$) were selected as instrumental variables, followed by LD clumping ($r^2 < 0.001$, window size 10,000 kb) to guarantee variant independence.

Pancreatic transcriptomic datasets GSE76894 (19 T2D patients and 84 healthy controls; training set) and GSE64998 (36 T2D patients and 32 healthy controls; validation set) were retrieved from the GEO database (https://www.ncbi.nlm.nih.gov/geo/). Gene expression values were normalized via the RMA algorithm, and inter-dataset batch effects were corrected using ComBat.

The PBMC scRNA-seq dataset GSE255566, comprising samples from 3 T2D patients and 3 healthy controls, was likewise obtained from GEO. Quality control

criteria included removal of cells with fewer than 200 or more than 6,000 detected genes, and exclusion of cells with mitochondrial gene fractions exceeding 20%; only cells passing all thresholds were retained for downstream analyses.

BPF target proteins were predicted by querying three complementary databases—SEA, SwissTargetPrediction, and SuperPred—using the BPF structure (PubChem CID: 78378). Pharmacokinetic profiling was conducted with SwissADME.

2.2 MR Analysis

Causal relationships between BPF exposure and T2D and its eight common complications were assessed using two-sample MR via the TwoSampleMR package (R version 4.3.0). The IVW method served as the primary estimator. Complementary sensitivity analyses employed MR-Egger regression, the weighted median estimator, simple mode, and weighted mode methods. Cochran's Q statistic evaluated instrument heterogeneity, while horizontal pleiotropy was examined through the MR-Egger intercept test and the MR-PRESSO global test (absence of pleiotropy defined as $P > 0.05$). Leave-one-out analyses quantified the contribution of each SNP to the overall causal estimate. Results were presented as scatter plots, forest plots, and funnel plots.

2.3 Differential Expression Gene Analysis

DEG analysis comparing T2D and healthy control pancreatic samples was conducted using the limma package (v3.62.1) in R, with thresholds set at $|FC| > 1$ and FDR-adjusted $P < 0.05$. DEG distribution was visualized with volcano plots generated

via ggplot2, and the expression patterns of the top 20 up- and downregulated genes were depicted in heatmaps constructed using pheatmap.

2.4 WGCNA

The WGCNA package (v1.72) was employed to construct a weighted gene co-expression network and delineate modules associated with T2D. A soft-thresholding power of $\beta = 5$ was determined based on scale-free topology criteria ($R^2 > 0.85$). The adjacency matrix was converted to a TOM, and hierarchical clustering was performed on the dissimilarity matrix (1-TOM). Modules were defined using the dynamic tree-cut algorithm (minimum module size: 30 genes; deep split: 3; merging threshold: 0.25). Module eigengenes were correlated with disease phenotype via Pearson analysis, and modules reaching significance ($P < 0.05$) were selected for hub gene extraction.

2.5 Integration of Candidate Target Genes

Candidate genes were obtained by computing the three-way intersection—using Venn diagrams—of: (1) DEGs from differential expression analysis, (2) hub genes from T2D-associated WGCNA modules, and (3) BPF-predicted target proteins. Overlapping genes were designated as candidate target genes for BPF-mediated T2D pathogenesis.

2.6 Functional Enrichment Analysis

Gene Ontology (GO) and Kyoto Encyclopedia of Genes and Genomes (KEGG) pathway enrichment analyses of candidate genes were carried out with the clusterProfiler package (v4.8.3), supplemented by Reactome pathway analysis. Terms

with FDR-adjusted $P < 0.05$ were considered statistically significant, and enrichment results were displayed as bar charts using ggplot2.

2.7 Protein-Protein Interaction Network Construction

PPI networks for candidate genes were generated via the STRING database (v11.5; https://cn.string-db.org/), applying a minimum interaction confidence threshold of 0.4. The resulting network was imported into Cytoscape (v3.9.1) for topological characterization, with key nodes prioritized by degree, betweenness, and closeness centrality metrics.

2.8 Machine Learning Screening of Core Genes

The randomForest package was applied (ntree = 500; mtry = $\sqrt{p}$). Genes were ranked by mean decrease in Gini impurity or mean decrease in accuracy, and top-ranked genes were selected as feature candidates. The xgboost package was run with parameters max_depth = 6, eta = 0.3, and nrounds = 100. Feature importance scores were used to prioritize candidate genes. LASSO Regression: Penalized logistic regression was implemented via the glmnet package, with the optimal regularization parameter λ chosen by 10-fold cross-validation (lambda.min or lambda.1se). Genes retaining non-zero coefficients at the selected λ were considered selected features. Core genes were defined as those consistently selected across all three algorithms.

2.9 Diagnostic Efficacy Assessment of Core Genes

The Wilcoxon rank-sum test was used to compare expression differences of core genes between T2D and control groups. Receiver operating characteristic (ROC) curve analysis was performed using the pROC package to calculate the area under the

curve (AUC) and its 95% confidence interval (CI) to assess the diagnostic efficacy of core genes. Validation was performed in both the training set (GSE76894) and independent validation set (GSE64998) to evaluate the robustness and generalization ability of diagnostic efficacy.

2.9 Diagnostic Efficacy Assessment of Core Genes

Expression differences of core genes between T2D and control groups were assessed by Wilcoxon rank-sum test. ROC curves were constructed using the pROC package, with AUC values and 95% CIs computed to quantify diagnostic performance. Analyses were replicated in both the training set (GSE76894) and independent validation set (GSE64998) to assess cross-cohort generalizability.

2.10 Single-Gene GSEA

GSEA was performed on core genes using clusterProfiler. Samples were stratified into high- and low-expression groups based on median core gene expression. KEGG pathway analysis yielded NES and nominal P-values; NES > 0 indicated pathway enrichment in the high-expression group, and NES < 0 indicated enrichment in the low-expression group. $P < 0.05$ was the significance threshold.

2.11 Single-Cell RNA Sequencing Data Analysis

ScRNA-seq data processing was performed with the Seurat package (v4.3.0). Post-QC data were normalized using LogNormalize (scale factor = 10,000), and the top 2,000 highly variable genes were identified by the vst method. After data scaling and linear transformation, PCA was conducted; the first 17 statistically significant

PCs ($P < 0.05$) were retained based on elbow and JackStraw plots. Cell clustering was performed using FindNeighbors and FindClusters (resolution = 0.5, Louvain algorithm), and UMAP was used for two-dimensional visualization. Cell types were annotated by canonical marker gene expression, corroborated by SingleR-based automated annotation and manual review. Intergroup differences in cell type proportions were evaluated using chi-square or Fisher's exact tests, and proportions were illustrated as bar charts via ggplot2. INSR expression was visualized across cell clusters using FeaturePlot and DotPlot.

Cell-cell communication was interrogated with the CellChat package (v1.6.1). Separate CellChat objects were constructed for T2D and healthy control groups. Communication probabilities were inferred from ligand, receptor, and cofactor expression profiles using the CellChatDB (human) interaction database. Significant ligand-receptor pairs ($P < 0.05$) were identified, and interaction numbers and strengths between cell types were quantified.

2.12 Drug Prediction and Molecular Docking

Putative therapeutic compounds were identified through CMAP (https://clue.io/) and DSigDB (http://tanlab.ucdenver.edu/DSigDB/). Candidate gene lists were submitted to CMAP, and core genes were queried in DSigDB; compounds with the most negative connectivity scores and greatest statistical significance were prioritized. Ligand 3D structures (SDF format) were downloaded from PubChem, and the INSR crystal structure was retrieved from PDB (https://www.rcsb.org/) or modeled using AlphaFold2 where necessary.

Molecular docking was performed with AutoDock Vina (v1.2.0). Protein and ligand preparation—including hydrogen addition and Gasteiger charge assignment—was conducted in AutoDockTools. The docking grid box was centered on the predicted binding pocket (exhaustiveness = 8). Binding free energy (kcal/mol) was used as the affinity metric, with more negative values reflecting stronger binding. Docking poses were visualized in PyMOL to characterize hydrogen bond and hydrophobic contact networks.

2.13 Statistical Analysis

All analyses were executed in R (v4.3.0). Non-normally distributed continuous variables were compared by Wilcoxon rank-sum test; normally distributed variables were assessed by Student's t-test. Categorical variables were evaluated with chi-square or Fisher's exact tests. Correlations were quantified using Pearson or Spearman coefficients as appropriate. Multiple testing correction applied the Benjamini-Hochberg FDR procedure. All reported P-values are two-tailed, with $P < 0.05$ regarded as statistically significant.

3 Results

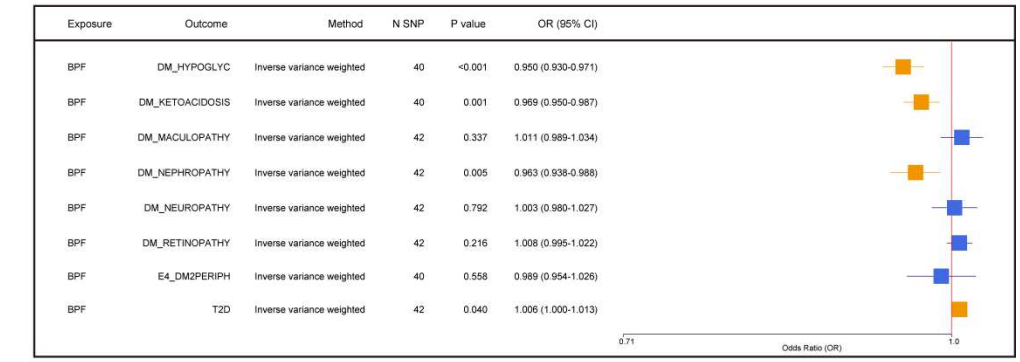
3.1 MR Analysis

For detailed information about BPF-related SNPs after following standard quality control procedures, see Supplementary Table S1. To evaluate the association between BPF and T2D and its common complications, we performed MR MR in European individuals. Using the IVW method as the main analysis method, the results showed

that only BPF was statistically significantly positively correlated with T2D (OR = 1.006, 95% CI: 1.000–1.013, P = 0.040) (Figure 1A). The remaining BPF were statistically significantly negatively correlated with DM_HYPOGLYC, DM_KETOACIDOSIS and DM_NEPHROPATHY, but failed to pass the horizontal multiplicity and sensitivity analysis. Therefore, T2D was selected as the key outcome. Scatter plots (Figure 1B) and forest plots (Figure 1C) showed that each SNP was significantly associated with BPF, indicating that BPF exposure was positively correlated with T2D. Sensitivity analyses, including heterogeneity assessment, horizontal pleiotropy and leave-one-out analysis, validated the preliminary MR analysis. MR analysis found no evidence of pleiotropy or heterogeneity between BPF and T2D, as shown by MR-Egger intercept test, MR-PRESSO global detection, Cochran's IVW and MR-Egger Q detection. In addition, in the "leave-one-out" analysis, the recalculated association estimates did not change significantly after removing any SNP, indicating that no individual SNP exerted a dominant influence on the overall causal estimate, thus confirming the robustness of the MR results (Figure 1D), while the funnel plot showed a nearly symmetric distribution, indicating the stability and reliability of the MR results (Figure 1E).

A

Exposure	Outcome	Method	N SNP	P value	OR (95% CI)
BPF	DM_HYPOGLYC	Inverse variance weighted	40	<0.001	0.950 (0.930-0.971)
BPF	DM_KETOACIDOSIS	Inverse variance weighted	40	0.001	0.969 (0.950-0.987)
BPF	DM_MACULOPATHY	Inverse variance weighted	42	0.337	1.011 (0.989-1.034)
BPF	DM_NEPHROPATHY	Inverse variance weighted	42	0.005	0.963 (0.938-0.988)
BPF	DM_NEUROPATHY	Inverse variance weighted	42	0.792	1.003 (0.980-1.027)
BPF	DM_RETINOPATHY	Inverse variance weighted	42	0.216	1.008 (0.995-1.022)
BPF	E4_DM2PERIPH	Inverse variance weighted	40	0.558	0.989 (0.954-1.026)
BPF	T2D	Inverse variance weighted	42	0.040	1.006 (1.000-1.013)



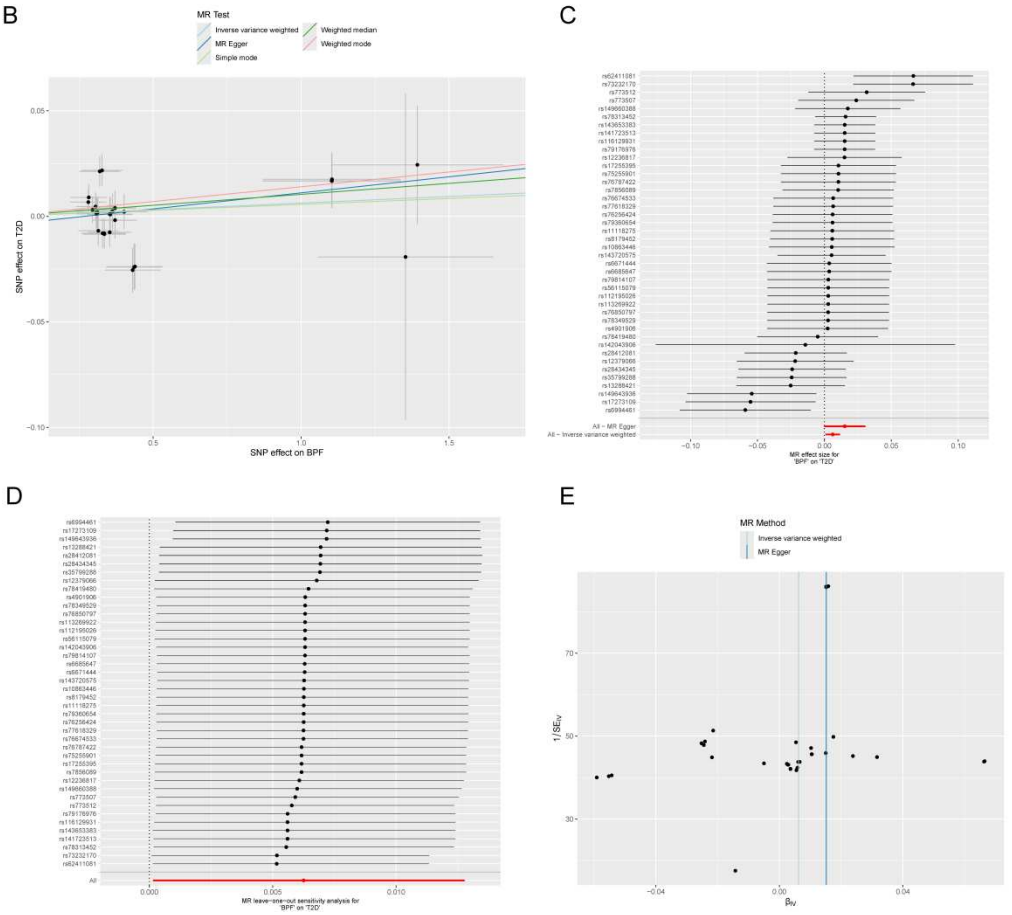


Figure 1 Potential association between BPF exposure and T2D and its common complications

(A) MR analysis results. (B) Scatter plot of forty-two SNPs applied five MR testing methods. (C) Forest plot of association between BPF and T2D risk. (D) Leave-one-out analysis for association between BPF and T2D. (E) Funnel plot for assessing symmetry in MR analysis.

3.2 Preliminary Exploration, Toxicity Characteristics and Impact Analysis of Bisphenol F

The absorption characteristics of BPF were evaluated based on the Swiss ADME database, where LIPO (lipophilicity), SIZE (molecular weight, MW), POLARITY, INSOLU (solubility), INSATU (unsaturation) and FLEX (flexibility) are key parameters for evaluating the physicochemical properties of compounds. The colored area represents the physicochemical space suitable for oral bioavailability. The analysis results show that BPF belongs to this area, indicating that BPF may have good oral absorption characteristics (Supplementary Figure 1).

3.3 Identification of Potential Targets and Pathways Associated with BPF Exposure in T2D

Integration of SEA, SwissTargetPrediction, and SuperPred databases yielded 212 putative BPF targets (Supplementary Figure 2). Differential expression analysis of GSE76894 identified 2,024 significantly altered genes in T2D pancreatic tissues relative to normal islets ($|FC| > 1$, adjusted $P < 0.05$), comprising 1,316 downregulated and 708 upregulated genes (Figure 2A). Volcano plots illustrated the bimodal separation of up- and downregulated DEGs, and heatmaps delineated the expression patterns of the 20 most significantly dysregulated genes in each direction across T2D and control samples (Figure 2B), revealing coherent inter-group expression differences suggestive of pathogenic relevance.

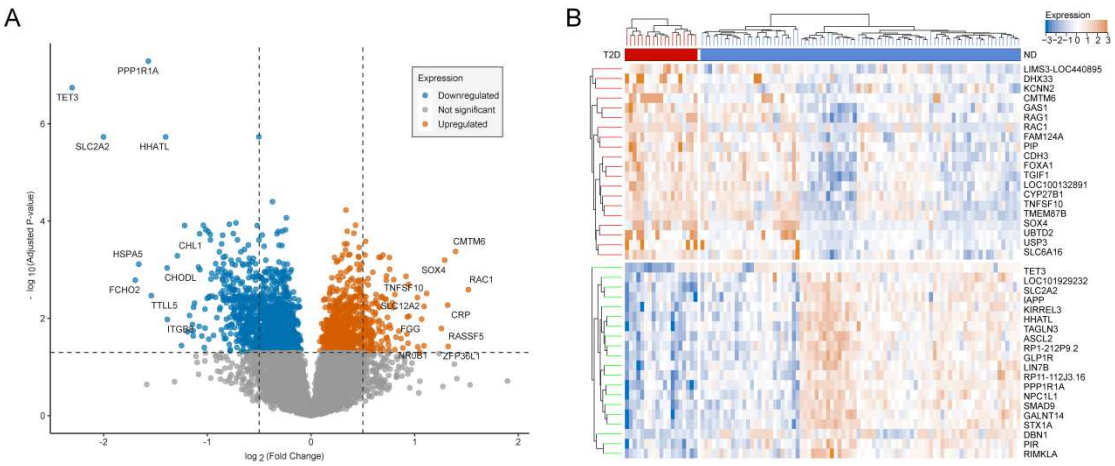


Figure 2. Identification of Core Differential Genes in T2D

(A) Volcano plot of differential analysis, red dots represent upregulated genes, blue dots represent downregulated genes, and black dots represent non-differential genes. (B) Heat map showing the expression patterns of the top 20 significantly upregulated and downregulated DEGs in T2D group and normal group (ND) samples.

WGCNA of the transcriptomic dataset selected $\beta = 5$ as the optimal soft-thresholding power for scale-free network construction (Figure 3A). Hierarchical clustering with dynamic tree-cutting (minimum module size: 30; deep split: 3; merging threshold: 0.25) resolved eight co-expression modules. Inter-module eigengene distances exceeded 0.25, confirming module independence (Figures 3B, C). Four modules—darkorange, brown, grey60, and turquoise—were significantly correlated with disease status ($P < 0.05$; Figure 3D), yielding 3,577 hub genes. Three-way intersection of DEGs, BPF targets, and WGCNA hub genes produced 11 candidate target genes (Figure 3E).

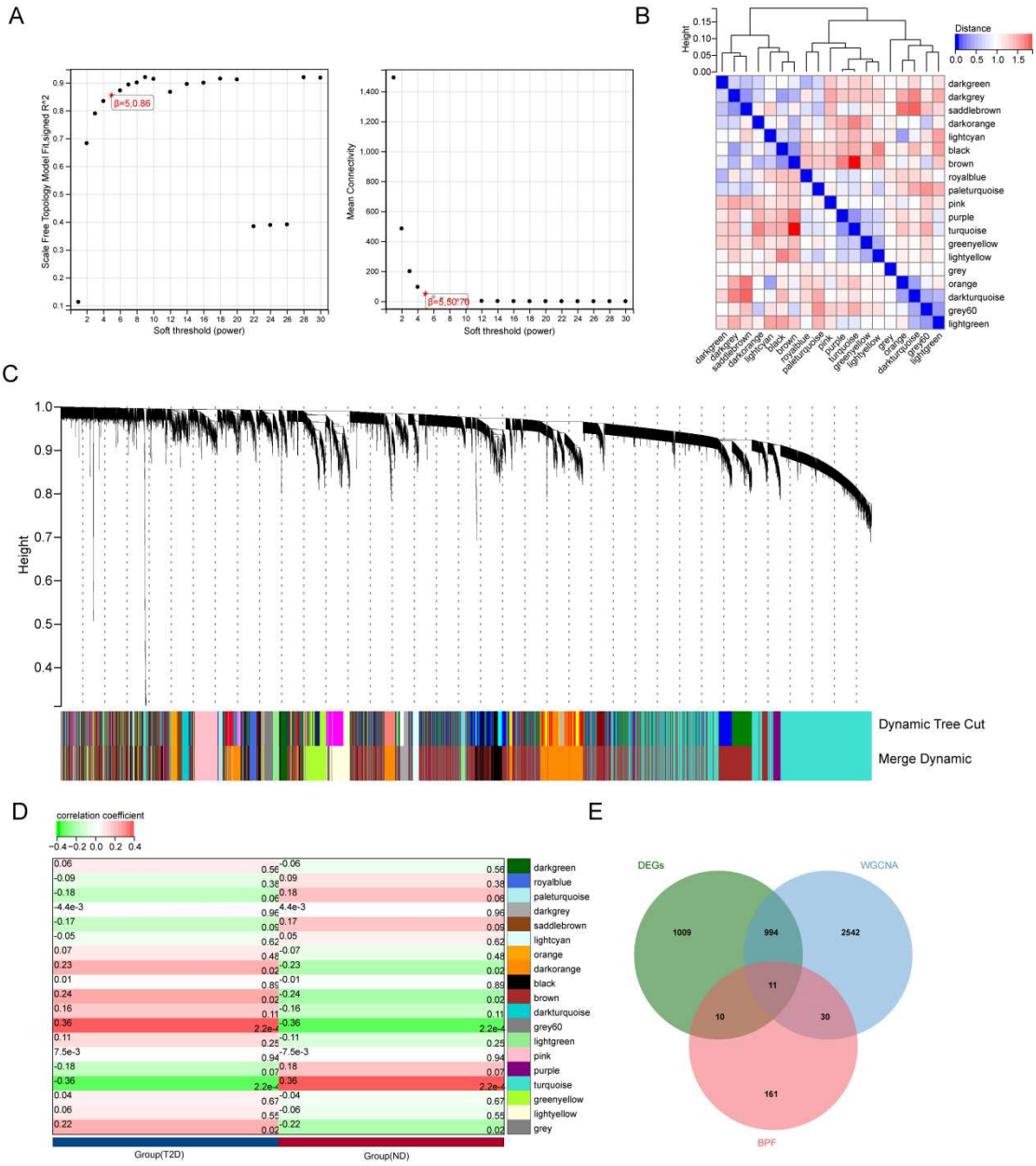


Figure 3.Identification of Core Pathogenic Targets in T2D

(A) Scale-free fit index and mean connectivity plots for soft-threshold selection. (B) Module eigengene clustering dendrogram. (C) Gene-module assignment diagram. (D) Module-trait correlation heatmap. (E) Venn diagram depicting the intersection of DEGs, WGCNA hub genes, and BPF targets.

3.4 Functional Enrichment Analysis Reveals Key Biological Processes and Pathways

GO analysis (Figure 4A) showed that in terms of biological processes, these genes were mainly enriched in regulation of potassium ion transport, positive regulation of glycogen biosynthetic process, regulation of glycogen metabolic process, positive regulation of glucose metabolic process and other processes; in terms of cellular components, they mainly involved neuron projection membrane, leading edge membrane, dendritic spine, basolateral plasma membrane and other structures; in terms of molecular functions, they participated in nuclear receptor activity, ligand-activated transcription factor activity, ligand-gated channel activity and other functions. KEGG pathway enrichment analysis (Figure 4B) showed that these genes were significantly enriched in Type II diabetes mellitus, Hormone signaling, Arachidonic acid metabolism, Prolactin signaling pathway, Insulin signaling pathway, cGMP-PKG signaling pathway, Neuroactive ligand signaling, Chemical carcinogenesis-receptor activation, Maturity onset diabetes of the young, Galactose metabolism and other pathways. PPI network analysis (Figure 4C) revealed the interaction relationships among candidate genes such as RORB, EPHX2, GRIA2, KCNH2, MAP1, ESR1, HPGD, ADRA2A, INSR, GCK.

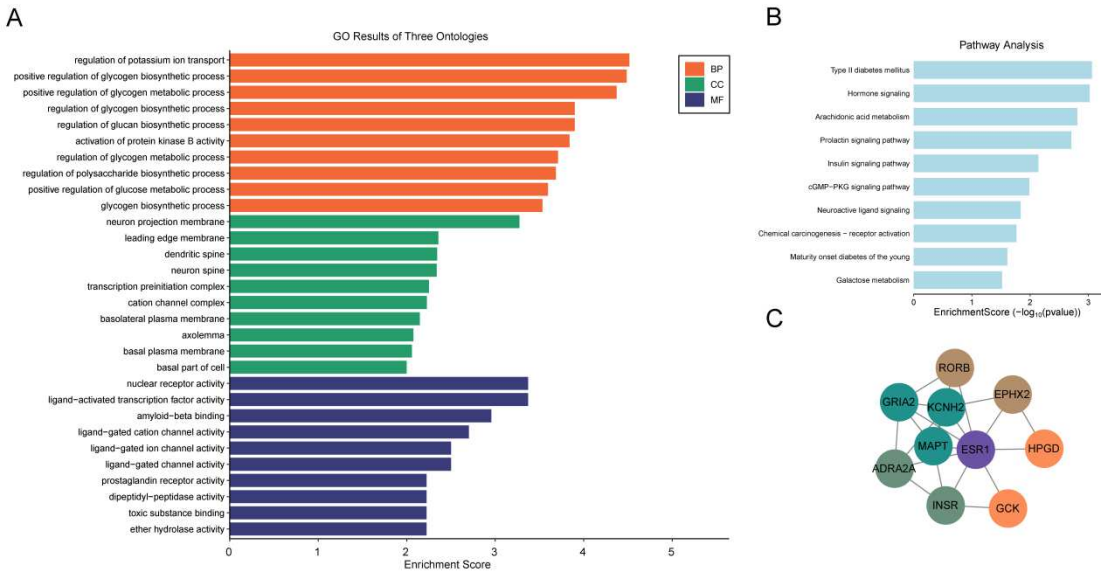


Figure 4. Candidate Gene Enrichment Analysis

(A) GO enrichment analysis; (B) KEGG enrichment analysis. (C) PPI network.

3.5 Core Gene Identification and Screening

Machine learning screening of the 11 candidate genes in the training set was performed sequentially. Random Forest analysis retained 1 feature gene (Figure 5A); XGBoost identified 6 feature genes (Figure 5B); and LASSO logistic regression selected 5 feature genes at the optimal λ (Figure 5C). The intersection of these three gene sets converged on INSR as the sole core gene (Figure 5D).

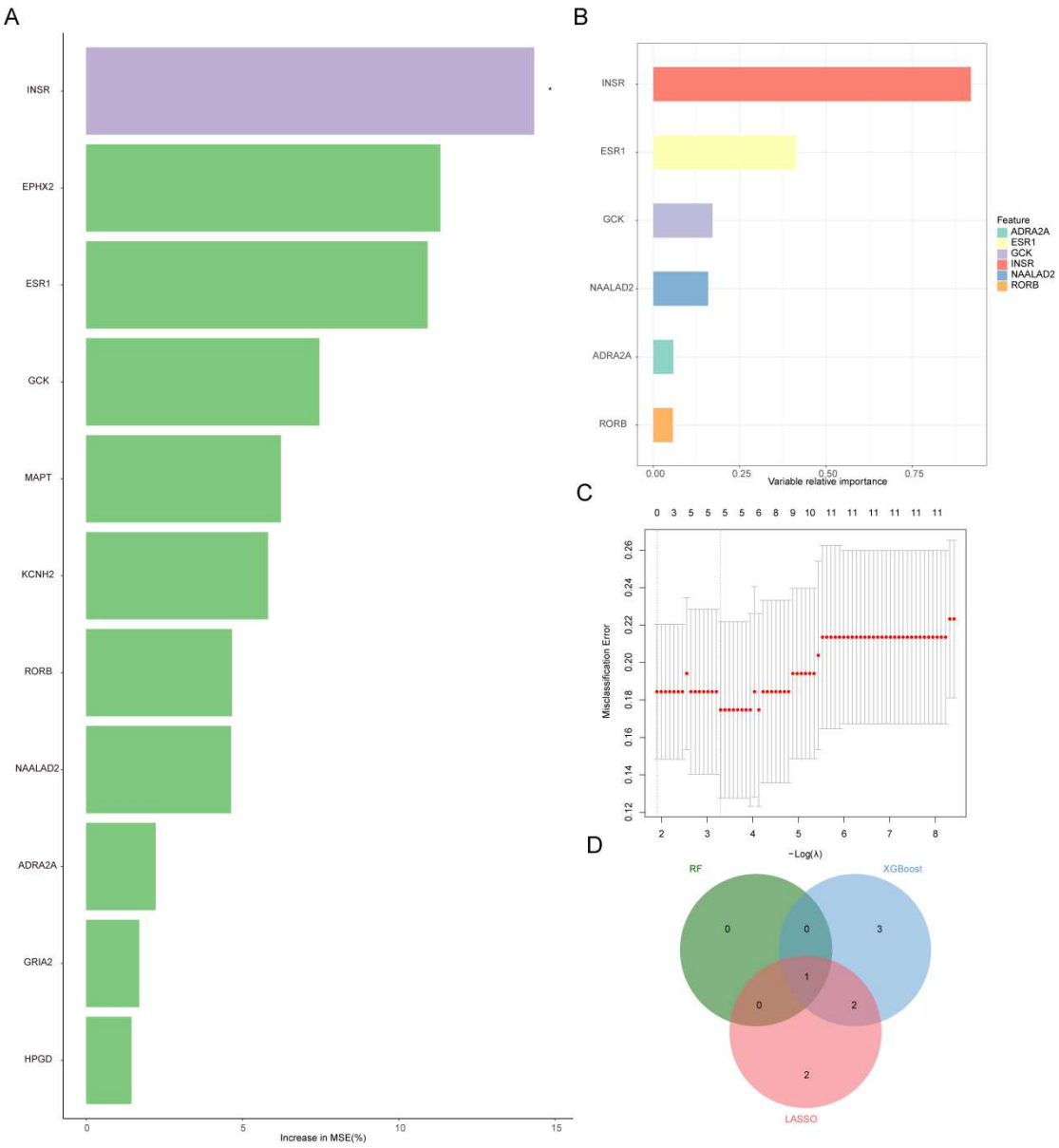


Figure 5. Core Gene Screening

(A) Random Forest feature importance ranking (sorted by MSE increase). (B) XGBoost feature importance analysis. (C) LASSO regularization path and gene selection at optimal λ. (D) Venn diagram showing convergence of three machine learning algorithms on INSR.

3.6 Single-gene GSEA Enrichment Analysis

To identify biological pathways related to key INSR gene expression, we performed single-gene GSEA analysis. The results (Figure 6) showed that INSR

exhibited significant positive enrichment in metabolic and signaling pathways, including apoptosis, insulin signaling pathway, etc., while it exhibited significant negative enrichment in long-term potentiation and oxidative phosphorylation pathways. In addition, this gene showed positive enrichment in multiple cancer-related pathways, including prostate cancer, acute myeloid leukemia, small cell lung cancer, chronic myeloid leukemia and pathways in cancer. In summary, these results reveal the multi-dimensional regulatory role of this gene in the pathogenesis of T2D: maintaining cellular energy homeostasis through participation in metabolic reprogramming such as pentose and glucuronate interconversions, mediating key signaling through insulin signaling pathway and ErbB signaling pathway, while the inhibitory effect on long-term potentiation and oxidative phosphorylation suggests its important role in regulating neuroplasticity and mitochondrial function.

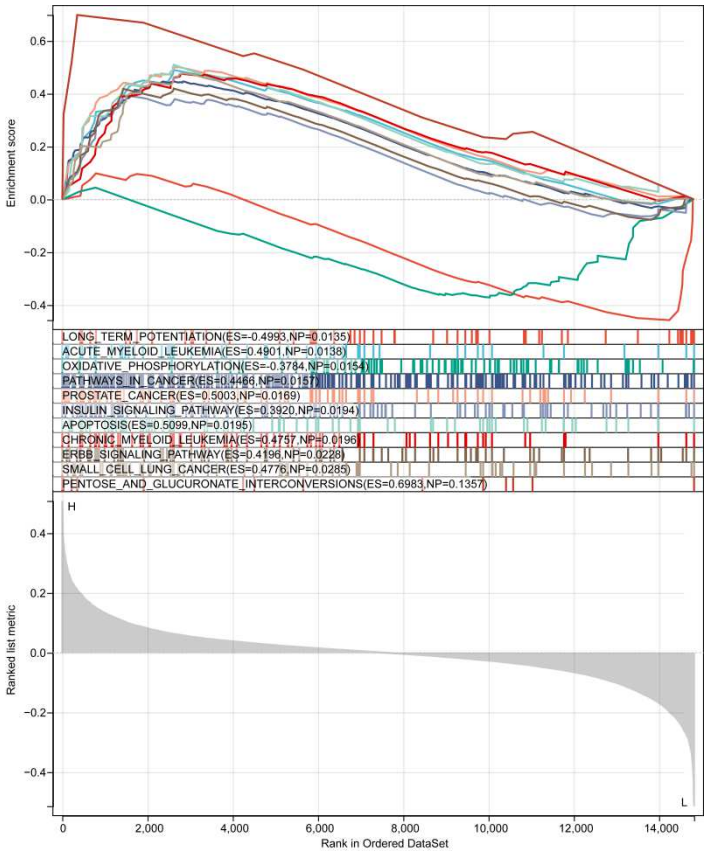


Figure 6. INSR Single-gene GSEA Enrichment Analysis

3.7 Core Gene Validation

INSR expression was significantly elevated in T2D relative to ND pancreatic samples in the training set ($P = 1.9\times10^{-5}$), and ROC analysis demonstrated excellent discriminatory capacity (AUC = 0.92, 95% CI: 0.70–0.93), with sensitivity and specificity both approaching 1.0 (Figure 7A). Independent validation in GSE64998 confirmed the upregulation of INSR in T2D ($P = 0.04$), with ROC analysis yielding an AUC of 0.82 (95% CI: 0.59–1.00) (Figure 7B). The consistent diagnostic performance across both cohorts supports the potential clinical utility of INSR as a T2D biomarker, while the modest AUC attenuation in the validation set likely reflects inter-cohort biological and sample heterogeneity.

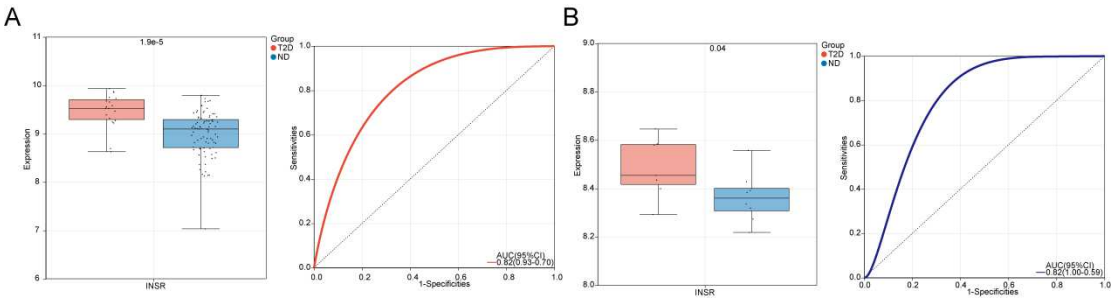


Figure 7 Expression Differences and Diagnostic Efficacy Evaluation of INSR in Training Set and Validation Set

(A) INSR expression comparison and ROC analysis in the training set (GSE76894). (B) INSR expression comparison and ROC analysis in the independent validation set (GSE64998).

3.8 Single-cell Data Analysis

ScRNA-seq analysis of GSE255566 was conducted to resolve INSR expression across immune cell subsets and characterize the T2D immune microenvironment. Following stringent QC and normalization, UMAP visualization revealed distinct transcriptomic clustering between T2D and control samples (Figure 8A). The first 17 statistically significant PCs were used for graph-based clustering, resolving 18 cell subpopulations, which were subsequently annotated into five major immune cell types—neutrophils, NK cells, monocytes, T cells, and B cells—based on canonical marker gene expression (Figures 8B, C). Cell composition analysis demonstrated a significant reduction in neutrophil frequency and concurrent expansion of NK cells, monocytes, T cells, and B cells in T2D peripheral blood relative to healthy controls (Figure 8D), indicative of systemic immune dysregulation linked to chronic metabolic inflammation.

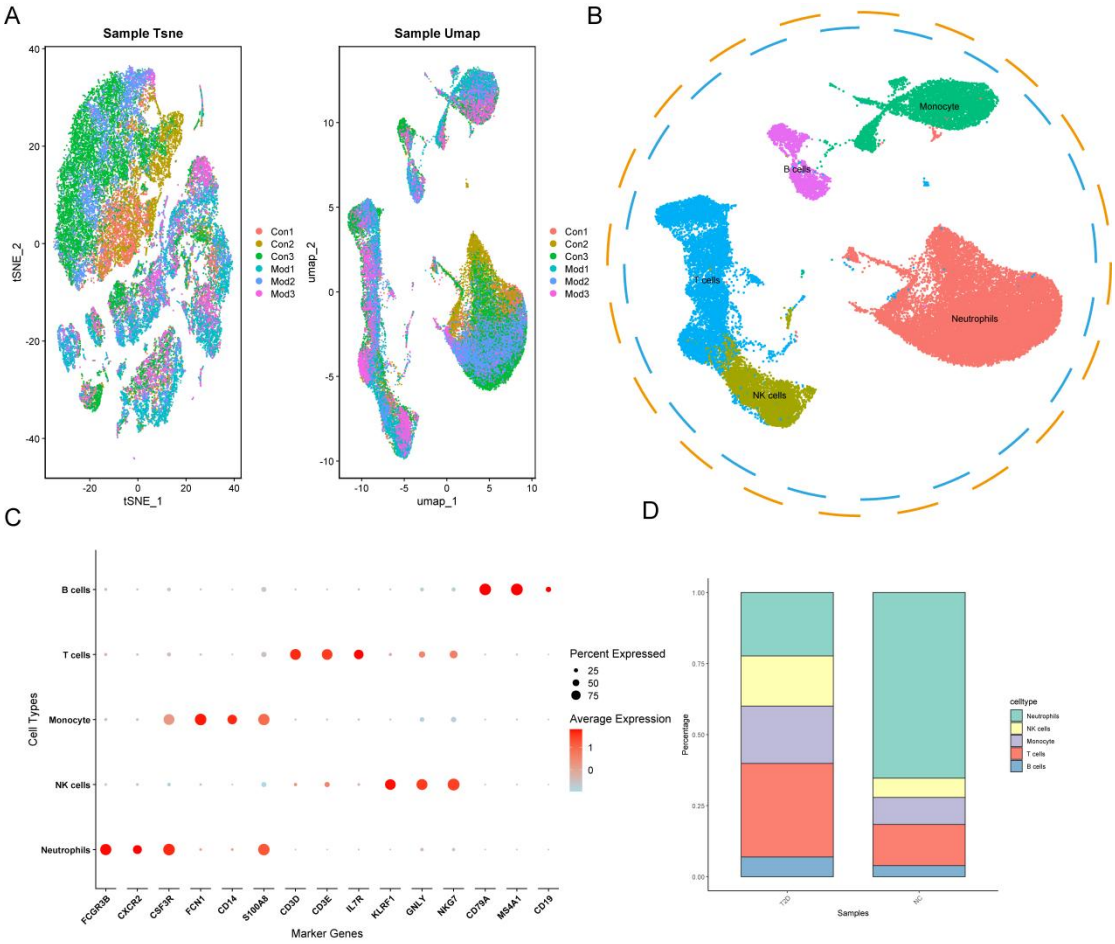


Figure 8 Single-cell Data Analysis

(A)Single-cell data dimensionality reduction clustering plot. (B) Cell annotation Umap plot. (C) Cell annotation marker dot plot. (D) Inter-group cell proportion bar plot.

UMAP visualization confirmed preferential INSR expression in monocytes (Figure 9A), and DotPlot quantification revealed that monocytes harbored the highest average INSR expression (mean = 1.5), substantially exceeding levels in NK cells, neutrophils, T cells, and B cells (Figure 9B). Intercellular communication network analysis demonstrated extensive cross-cellular interactions, with NK cells engaging broadly with other immune subsets, while monocytes, neutrophils, T cells, and B cells collectively formed a dense signaling network (Figure 9C). CellChat analysis

identified divergent outgoing and incoming INSR-related signaling profiles across cell types (Figure 9D), consistent with multi-pathway INSR-mediated immune regulation. Among the top 20 ligand-receptor pairs associated with monocytes, IGF1-INSR and IGF1-IGF1R occupied dominant positions across the monocyte-T cell and monocyte-NK cell communication axes (Figure 9E). Additional signaling families—including VEGFA, CXCL, and HLA-C—contributed to a layered intercellular network. Bidirectional signaling was prominent for CLEC2D-KLRB1 and HLA-E-KLRK1 pairs, whereas MIF-associated pathways predominantly operated as signal emitters (Figure 9F). The global communication landscape confirmed the strongest interaction intensity between monocytes and neutrophils, with notable monocyte-NK cell crosstalk also evident (Figure 9G). These findings position monocytes as the principal signaling hub and neutrophils as key communication partners within the INSR-centered immune network in T2D.

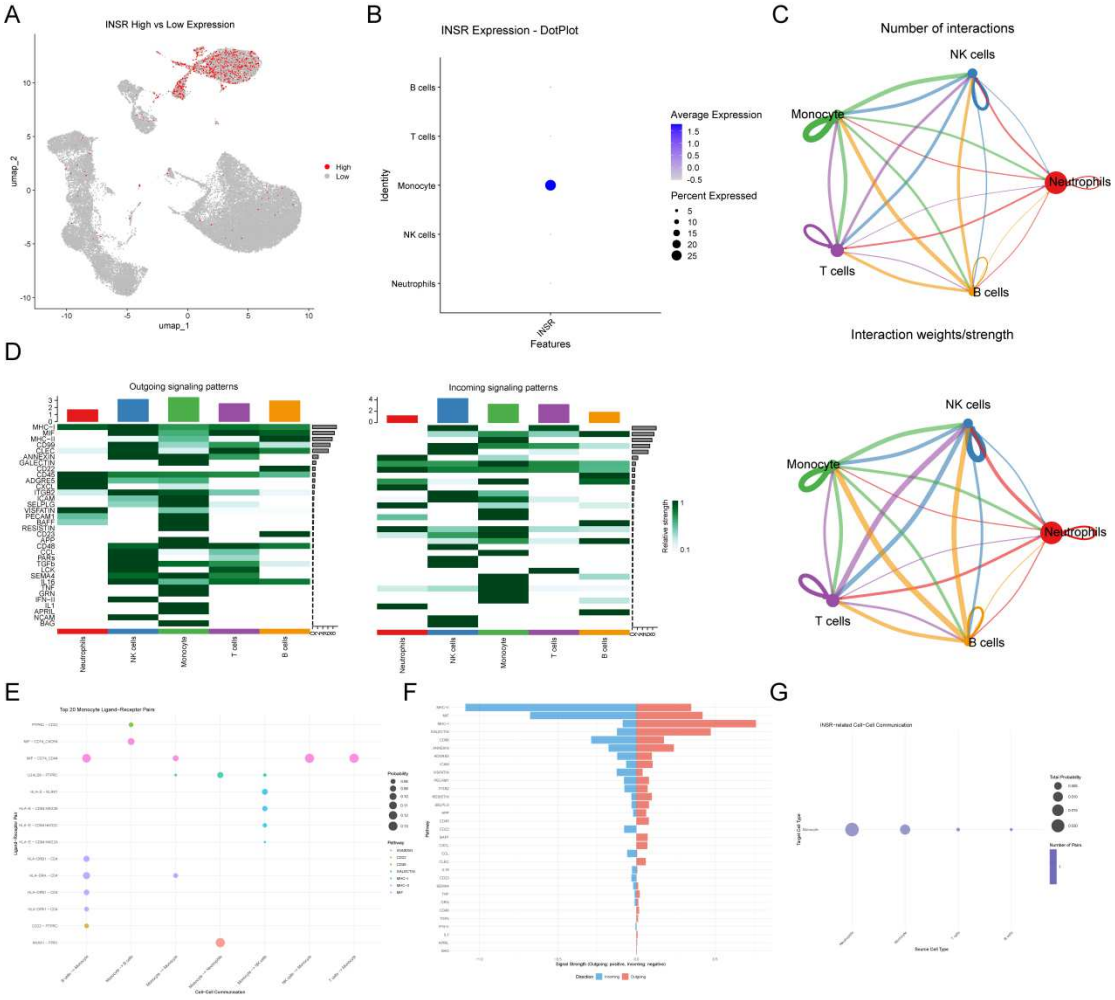


Figure 9 INSR expression distribution and intercellular communication network analysis in peripheral blood immune cells

(A) UMAP feature plot of INSR expression across immune cell subpopulations. (B) DotPlot quantifying mean INSR expression and expressing cell fraction across five cell types. (C) Circle plot of intercellular interaction networks. (D) Outgoing and incoming signaling pathway profiles for each cell type. (E) Bubble plot of the top 20 ligand-receptor pairs associated with monocyte communication. (F) Signal strength and directionality of monocyte-associated ligand-receptor pairs. (G) Chord diagram of the overall intercellular communication landscape.

3.9 Molecular Docking and Dynamics Simulation

Molecular docking revealed favorable binding affinity between BPF and the INSR protein ($\Delta G = -6.7$ kcal/mol; Supplementary Table 1). BPF occupied the ligand-binding pocket defined by key residues Tyr232, Met56, and Ala227, engaging the protein via multiple hydrogen bonds and hydrophobic contacts (Figures 10A, B), providing a structural rationale for BPF-mediated perturbation of insulin receptor function.

To assess complex stability, 100 ns MD simulations were conducted on the top-ranked BPF-INSR docking pose using GROMACS 2021 with the Amber14SB force field (Supplementary Table 2). RMSD values stabilized early in the simulation at approximately 0.7 nm (Figure 10C), Rg remained constant throughout (Figure 10D), and SASA decreased progressively (Figure 10E), collectively indicating a compact and conformationally stable complex over the simulation period. Together, docking and MD simulation data provide convergent computational evidence for a direct and stable BPF-INSR interaction.

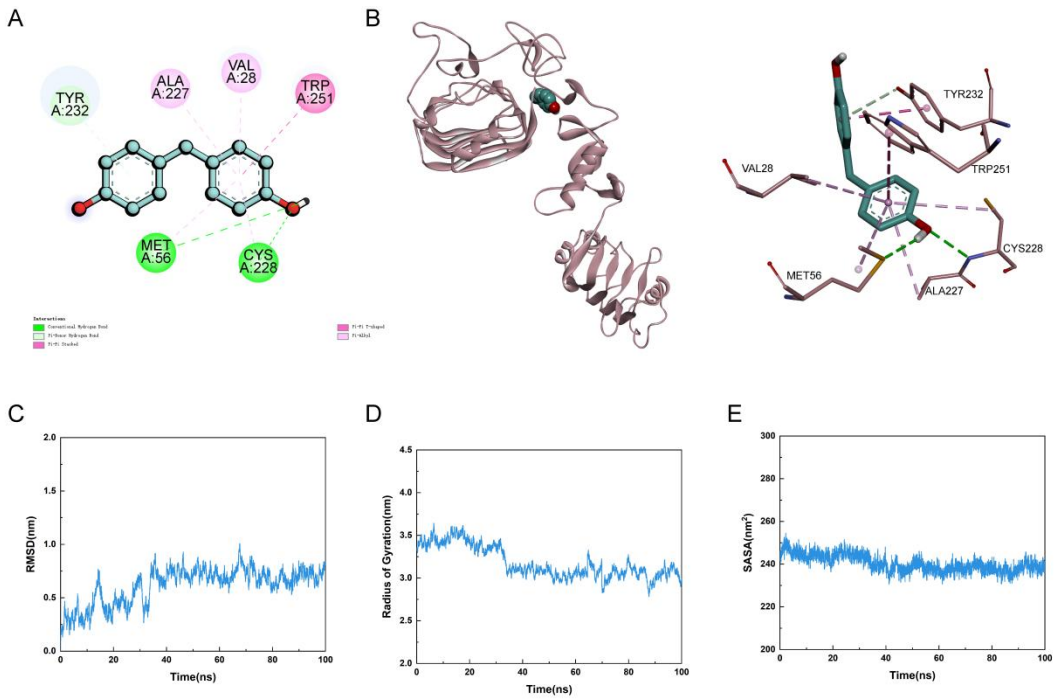


Figure 10 Molecular docking and molecular dynamics simulation of the BPF-INSR complex

(A–B) Three-dimensional visualization of BPF binding mode within the INSR ligand-binding pocket. (C–E) Time-course plots of RMSD (C), radius of gyration Rg (D), and solvent accessible surface area SASA (E) for the BPF-INSR complex during 100 ns MD simulation.

4 Discussion

T2D is emerging as a critical global health challenge, driven by a complex interplay between genetic predisposition and environmental factors[13] BPA, a prototypical endocrine-disrupting chemical, is well-established as a contributor to insulin resistance and T2D[14]. However, as restrictions on BPA tighten, BPF has emerged as a primary substitute, raising new safety concerns[15]. While previous observational studies have suggested an association between urinary BPF levels and dysglycemia, establishing causality has been hindered by potential confounding factors[16]. By employing a two-sample MR analysis based on large-scale GWAS data,

we confirmed at the genetic level that BPF exposure is an independent risk factor for T2D (OR = 1.006). Although the observed OR value appears modest, it is consistent with effect sizes typically reported in MR studies of environmental exposures, where genetic instruments capture only a fraction of total exposure variance[17]. Moreover, given the ubiquitous and chronic nature of BPF exposure in modern populations, even small individual-level risks can translate into substantial population-attributable fractions. This finding supports the hypothesis that BPF possesses metabolic toxicity[18]. Our results align with recent findings by Li *et al.* regarding BPF-induced hepatic lipid metabolism disorders[19], underscoring the urgent need to reassess public health exposure limits for this ubiquitous environmental contaminant.

In this study, we systematically elucidated the causal relationships and underlying molecular mechanisms connecting exposure to the environmental endocrine disruptor BPF with T2D by integrating MR, multi-omics analysis, and molecular dynamics simulations. Our results provide converging computational evidence that BPF exposure is causally associated with an increased risk of T2D and identify the INSR as a critical core target mediating this pathogenic process. Furthermore, single-cell transcriptomic analysis highlighted the preferential expression of INSR in monocytes and its pivotal role in modulating the immune microenvironment via the IGF1 signaling pathway. Collectively, our findings shed new light on how environmental BPF exposure drives metabolic dysfunction, and point to INSR as a potential biomarker for early risk stratification of T2D.

Our multi-omics enrichment analysis revealed that the disturbances induced by

BPF are specifically clustered within particular functional modules. Among these, hormone signaling as a major disrupted pathway, a finding consistent with the known endocrine-disrupting properties of BPF. As a structural analog of BPA and 17β-estradiol, BPF contains two phenol rings, enabling it to function as a potent EDC[20]. At the receptor level, it primarily acts as a xenoestrogen, binding both estrogen receptors and the membrane-bound G-protein coupled estrogen receptor (GPER)[21]. Physiologically, endogenous estrogen signaling contributes to the maintenance of glucose homeostasis. It supports the survival of pancreatic β-cells against oxidative stress, enhances glucose-stimulated insulin secretion, and improves insulin sensitivity in peripheral tissues (such as the liver and skeletal muscle) by modulating GLUT4 translocation[22]. However, exposure to BPF disrupts this delicate equilibrium through "molecular mimicry." By occupying estrogen receptors, BPF can initiate abnormal non-canonical signaling or act as an antagonist, thereby inhibiting the protective effects of endogenous estradiol.

Building on the identification of hormonal signaling disruption as an upstream event, we next sought to identify the specific molecular target through which BPF exerts its most direct downstream metabolic effects. Through the intersection of WGCNA and three machine learning algorithms, we pinpointed INSR as the core gene driving BPF-induced T2D. It is not only involved in metabolic regulation but serves as the essential regulator of systemic glucose homeostasis[23], representing the exclusive entry point for insulin signaling. The binding of insulin to the INSR α-subunit and the subsequent autophosphorylation of the β-subunit are the

rate-limiting steps that trigger the PI3K/Akt cascade, ultimately driving GLUT4 translocation and glucose uptake in peripheral tissues[24]. Therefore, any structural or functional impairment of INSR constitutes a defining event in the development of insulin resistance. Our molecular docking simulation offers structural evidence for BPF-induced insulin resistance. BPF was found to bind stably within the binding pocket of the INSR protein, interacting with key amino acid residues—such as Tyr232, Met56, and Ala227—via multiple hydrogen bonds and hydrophobic interactions. Notably, these residues are located within the ligand-binding domain of the INSR α-subunit, a region critical for insulin recognition and subsequent conformational changes that trigger β-subunit autophosphorylation[25]. Tyr232, in particular, has been implicated in stabilizing the insulin-receptor complex, and its occupation by BPF would directly interfere with proper receptor activation[26]. This binding mode results in a steric blockade: by occupying the critical binding pocket, BPF hinders the conformational changes requisite for receptor autophosphorylation. Unlike previous studies indicating that BPA primarily interferes with the phosphorylation of insulin receptor substrates[27], our findings suggest that BPF may act further upstream at the receptor level, representing a distinct and potentially more fundamental mechanism of metabolic disruption. Looking forward, we propose that INSR-binding potential be incorporated into the toxicological profiles of emerging bisphenol analogs (BPF, BPS, BPAF) to predict their diabetogenic risk prior to widespread industrial application.

Emerging evidence indicates a complex crosstalk between Estrogen Receptors and the Insulin Receptor, an interaction potentially disrupted by BPF[24, 27]. At the

molecular level, ER-α can physically interact with INSR and insulin receptor substrate-1 (IRS-1), forming a signaling complex that enhances insulin sensitivity in target tissues[28]. Estradiol binding to ER-α promotes the recruitment of phosphatidylinositol 3-kinase (PI3K) to the INSR-IRS-1 complex, thereby amplifying downstream Akt signaling and glucose transporter translocation[29]. Additionally, genomic ER signaling upregulates the transcription of key insulin signaling components, including INSR itself and glucose transporter genes[30]. By simultaneously altering the estrogenic milieu and directly interacting with INSR—as demonstrated in our molecular docking simulations—BPF exerts a dual impact on metabolic homeostasis. This "double-hit" mechanism—wherein BPF both disrupts ER-mediated enhancement of insulin signaling and directly blocks INSR function—may explain why bisphenol-induced metabolic dysfunction is often more severe than that caused by isolated defects in either pathway alone. This synergistic toxicity may accelerate the progression from impaired glucose tolerance to overt T2D.

A key observation from our research is the marked upregulation of INSR expression among T2D patients, which yielded a high diagnostic AUC of 0.83. This elevated AUC suggests that INSR expression can effectively differentiate T2D patients from healthy individuals, indicating that INSR functions not only as a signaling component but also as a promising clinical biomarker. While current diagnostic approaches for T2D predominantly rely on HbA1c and fasting glucose levels[31], INSR expression provides insight into the underlying etiology—specifically, receptor dysfunction. We hypothesize that heightened INSR expression may delineate

a distinct “BPF-Associated T2D Subtype.” This compensatory upregulation likely represents a cellular attempt to overcome functional receptor blockade induced by environmental toxicants[32]. However, increased receptor quantity cannot compensate for qualitative impairment in ligand binding or conformational activation, resulting in a state of “receptor resistance” analogous to the well-characterized phenomenon of insulin resistance[33]. Individuals with this profile might exhibit reduced responsiveness to conventional insulin-sensitizing therapies that target downstream pathways. Instead, they may benefit from interventions aimed at displacing environmental toxins from the receptor or stabilizing its structural conformation. This hypothesis warrants further investigation through prospective cohort studies that stratify T2D patients by environmental exposure history and INSR expression profiles. The diagnostic performance supports the utility of INSR as a novel biomarker, particularly for identifying patients whose insulin resistance is linked to environmental pollutant exposure, such as BPF, rather than solely to excessive caloric intake.

Having characterized the molecular basis of BPF–INSR interaction, we next extended our analysis to the cellular level to examine whether BPF-associated INSR dysregulation reshapes the peripheral immune landscape in a manner that could amplify metabolic inflammation in T2D. Building on the established link between T2D and chronic low-grade inflammation[34]. Our single-cell analysis demonstrated a profound restructuring of the peripheral immune landscape, characterized by a marked depletion of neutrophils alongside a relative expansion of monocytes and

lymphocytes. Although neutrophils are traditionally associated with acute inflammation[35, 36], their depletion here likely reflects immune exhaustion or toxicity-induced apoptosis. Given that bisphenols are known bone marrow toxicants[37], this reduction suggests that BPF may impair granulopoiesis or accelerate neutrophil turnover via oxidative stress. For individuals with T2D, this signifies not a reduction in inflammation, but rather an impairment of innate immunity[38, 39]. A compromised neutrophil count weakens the first line of defense against infection and suggests a systemic failure in immune cell maintenance[40].

In parallel with neutrophil depletion, the concurrent expansion of monocytes—the cell population we identified as harboring the highest INSR expression—points to a compositional shift in the immune landscape with distinct metabolic implications. This finding places monocytes at the epicenter of immunometabolism. Monocytes rely substantially on insulin signaling to drive glycolysis, which fuels their migratory and phagocytic functions[41]. The upregulation of INSR in monocytes from T2D patients likely represents a compensatory adaptation to systemic insulin resistance and potential BPF-mediated interference[42]. Due to their high INSR expression, monocytes serve as primary targets for BPF in circulation. The binding of BPF to monocyte INSR disrupts their metabolic programming, potentially causing these metabolically dysregulated monocytes to preferentially differentiate into pro-inflammatory M1 macrophages or foam cells[43]. This mechanism directly connects environmental BPF exposure to accelerated atherosclerosis, as these aberrant monocytes infiltrate vascular walls and initiate plaque formation[44].

Furthermore, our CellChat analysis identified the IGF1-INSR ligand-receptor pair as a key communication pathway, with monocytes functioning as a central signaling hub. IGF1 is structurally homologous to insulin and can activate signaling through INSR, particularly the INSR-A isoform[45]. This axis delivers vital survival and anti-apoptotic signals to immune cells, especially neutrophils[46]. This provides a key pathological insight into the observed neutrophil depletion: if BPF structurally obstructs or alters INSR conformation—as suggested by our molecular docking results—it effectively severs IGF1-INSR communication. The IGF1-INSR axis is essential for neutrophil survival, as IGF1 binding to INSR activates the IRS1/PI3K/Akt/FOXO1 pathway, which phosphorylates and inactivates pro-apoptotic proteins such as Bad and FoxO transcription factors[47, 48]. Disruption of this survival signaling renders neutrophils vulnerable to spontaneous apoptosis, particularly under conditions of metabolic stress characteristic of T2D[49, 50]. Consequently, neutrophils deprived of IGF1-mediated survival signals experience accelerated apoptosis, accounting for their reduced frequency in our dataset. In a compensatory yet ineffective feedback loop, monocytes increase INSR expression and secrete more IGF1, creating a state of "compensatory hyperactivation" that drives monocytes toward a hyper-inflammatory phenotype. This proposed mechanism establishes an “environmental toxin-immune metabolism-tissue injury” cascade may represent a critical mechanism accelerating the progression of diabetic complications, including cardiovascular pathologies.

In summary, this research establishes a multidimensional framework linking BPF

exposure to the pathogenesis of T2D and its cardiovascular complications. We propose that BPF elevates T2D risk by directly interacting with the INSR protein, thereby disrupting insulin signaling and modifying the immune communication axis between monocytes and neutrophils. Consequently, INSR is recognized not only as a central node within the BPF-induced diabetogenic network but also as a candidate diagnostic biomarker for environmentally induced metabolic disorders. It should be noted, however, that the designation of INSR as a biomarker remains provisional at this stage and requires prospective clinical validation before any diagnostic utility can be established.

Several limitations warrant consideration. First, our reliance on retrospective public datasets introduces inherent heterogeneity. While rigorous normalization procedures were applied to mitigate batch effects, intrinsic biological and technical variations across cohorts cannot be entirely eliminated. Additionally, the scRNA-seq component was limited by a relatively small sample size. Second, although MR provides a robust framework for causal inference, its validity is contingent upon the assumptions of the genetic instruments used, and the potential influence of horizontal pleiotropy cannot be entirely excluded. Third, while our molecular docking simulations predict stable BPF-INSR binding, these computational models require experimental validation through techniques such as surface plasmon resonance or isothermal titration calorimetry to confirm binding affinity and kinetics. Fourth, the proposed BPF-associated T2D subtype remains a hypothesis requiring validation in prospective cohorts with documented environmental exposure profiles and

longitudinal metabolic monitoring. Therefore, the computational predictions generated herein necessitate subsequent validation via definitive experimental approaches. Finally, while our research delineates a plausible mechanism of toxicity, it does not establish a definitive exposure threshold. It remains uncertain whether chronic, low-level environmental exposure to BPF is sufficient to induce the structural perturbations in INSR observed in our models, or whether these toxic effects follow a strictly dose-dependent relationship.

Future studies should prioritize validating INSR as a clinical biomarker in large-scale prospective cohorts, especially in populations with documented environmental exposure to bisphenols. Such studies should incorporate standardized BPF exposure measurements, longitudinal metabolic endpoints, and adjustment for relevant confounders to strengthen causal inference. Experimental investigations using animal models and cell lines are crucial to confirm the BPF-INSR interaction and its effects on monocyte-driven inflammation and glucose metabolism. In particular, dose-response experiments across physiologically relevant BPF concentrations are needed to address the exposure threshold question identified above. Moreover, exploring the therapeutic potential of targeting the IGF1-INSR axis may provide new strategies for managing T2D and its complications in the context of environmental pollution. Should the BPF-INSR interaction be experimentally confirmed, small-molecule or antibody-based interventions targeting this axis could represent a novel therapeutic avenue worth exploring. Extending this analytical approach to other environmental toxins could further reveal the complex etiology of

T2D.

Data Availability

All datasets used in this study are publicly available. GWAS summary statistics for T2D and its complications were obtained from the FinnGen database (https://www.finngen.fi/), while genetic variants associated with BPF exposure were retrieved from the GWAS Catalog (https://www.ebi.ac.uk/gwas/). Transcriptomic datasets GSE76894 and GSE64998, as well as the PBMC single-cell RNA-seq dataset GSE255566, were downloaded from the Gene Expression Omnibus (GEO) database (https://www.ncbi.nlm.nih.gov/geo/). The molecular structure of BPF (CID: 78378) was obtained from PubChem (https://pubchem.ncbi.nlm.nih.gov/).

Author Contributions

JT conceived, designed and supervised the study. YY performed the key bioinformatics analyses, interpreted the main findings, and drafted the manuscript. YF collected and processed the data, and contributed to drafting the manuscript. ZZ and WD assisted with bioinformatics analyses and results interpretation. SH validated the findings. ZZ and WD performed the molecular docking experiments. YF and SH provided critical feedback and helped shape the research. JT revised the manuscript and acquired the funding. All authors discussed the results and approved the final manuscript.

Acknowledgments

We would like to express our sincere gratitude to all the participants for their

contributions to this study.

Conflicts of Interest

The authors declare no conflicts of interest related to this study.

Funding

This work was supported by the Science and Technology Program of Jiangxi Provincial Administration of Traditional Chinese Medicine (Grant No. 2024B0910).

References:

[1] Magliano D J, Boyko E J, committee I D F D A t e s, 'IDF Diabetes Atlas', in *Idf diabetes atlas* (Brussels: International Diabetes Federation
© International Diabetes Federation, 2021., 2021).

[2] Tan M H P, Ong S C, Bujang M A, et al. Evaluation of the health-related quality of life of patients with type 2 diabetes in relation to macrovascular and microvascular complications[J]. Acta Diabetol, 2023, 60(12): 1735-1747.

[3] Kolarić V, Svirčević V, Bijuk R, et al. CHRONIC COMPLICATIONS OF DIABETES AND QUALITY OF LIFE[J]. Acta Clin Croat, 2022, 61(3): 520-527.

[4] Liu B, Lehmler H J, Sun Y, et al. Association of Bisphenol A and Its Substitutes, Bisphenol F and Bisphenol S, with Obesity in United States Children and Adolescents[J]. Diabetes Metab J, 2019, 43(1): 59-75.

[5] Sen A, Heredia N, Senut M C, et al. Multigenerational epigenetic inheritance in humans: DNA methylation changes associated with maternal exposure to lead can be transmitted to the grandchildren[J]. Sci Rep, 2015, 5: 14466.

[6] Ziegler D. Type 2 diabetes as an inflammatory cardiovascular disorder[J]. Curr Mol Med, 2005, 5(3): 309-22.

[7] Girard D, Vandiedonck C. How dysregulation of the immune system promotes diabetes mellitus and cardiovascular risk complications[J]. Front Cardiovasc Med, 2022, 9: 991716.

[8] Berbudi A, Khairani S, Tjahjadi A I. Interplay Between Insulin Resistance and Immune Dysregulation in Type 2 Diabetes Mellitus: Implications for Therapeutic Interventions[J]. Immunotargets Ther, 2025, 14: 359-382.

[9] Liu Z, Lu Y, Zhong K, et al. The associations between endocrine disrupting chemicals and markers of inflammation and immune responses: A systematic review and meta-analysis[J]. Ecotoxicol Environ Saf, 2022, 234: 113382.

[10] Merrill A K, Sobolewski M, Susiarjo M. Exposure to endocrine disrupting chemicals impacts immunological and metabolic status of women during pregnancy[J]. Mol Cell Endocrinol, 2023, 577: 112031.

[11] Barrett T, Wilhite S E, Ledoux P, et al. NCBI GEO: archive for functional genomics data sets--update[J]. Nucleic Acids Res, 2013, 41(Database issue): D991-5.

[12] Stuart T, Butler A, Hoffman P, et al. Comprehensive Integration of Single-Cell Data[J]. Cell, 2019, 177(7): 1888-1902.e21.

[13] Wang Y, Chen S, Li Y, et al. Metabolic profiling of frailty, associations with type 2 diabetes and interaction with genetic susceptibility[J]. Cardiovasc Diabetol, 2025, 24(1): 226.

[14] Della Rocca Y, Traini E M, Diomede F, et al. Current Evidence on Bisphenol A Exposure and the Molecular Mechanism Involved in Related Pathological Conditions[J]. Pharmaceutics, 2023, 15(3)

[15] Sun W, Guo Y, Sun X, et al. Alternatives Exert Higher Health Risks than Bisphenol A on Indo-Pacific Humpback Dolphins[J]. Environ Sci Technol, 2024, 58(1): 63-74.

[16] Peng J, Du L L, Ma Q L. Serum glycolipids mediate the relationship of urinary bisphenols with NAFLD: analysis of a population-based, cross-sectional study[J]. Environ Health, 2023, 21(1): 124.

[17] Burgess S, Davey Smith G, Davies N M, et al. Guidelines for performing Mendelian randomization investigations: update for summer 2023[J]. Wellcome Open Res, 2019, 4: 186.

[18] Shao Y, Zhu L, Chen Z, et al. Evidence of increased estrogenicity upon metabolism of Bisphenol F - Elucidation of the key metabolites[J]. Sci Total Environ, 2021, 787: 147669.

[19] Li Z, Wu Y, Qian M, et al. Multi-omics analysis reveals BPF exposure causes hepatic glucose and lipid metabolism disorder in rats by disrupting energy homeostasis[J]. Toxicology, 2025, 515: 154130.

[20] Huo S, Li B, Du J, et al. Neurotoxic effects of perinatal exposure to Bisphenol F on offspring mice[J]. Environ Pollut, 2024, 362: 124932.

[21] Liu X, Xue Q, Zhang H, et al. Structural basis for molecular recognition of G protein-coupled estrogen receptor by selected bisphenols[J]. Sci Total Environ, 2021, 793: 148558.

[22] Yang X, Dai K, Wang S. Genistein Enhances GLUT4 Expression and Translocation in the Gastrocnemius Muscle and Improves Systemic Glucose Metabolism in Ovariectomized Mice[J]. Nutrients, 2025, 17(17)

[23] Grandl G, Collden G, Feng J, et al. Global, neuronal or β cell-specific deletion of inceptor improves glucose homeostasis in male mice with diet-induced obesity[J]. Nat Metab, 2024, 6(3): 448-457.

[24] Su J, Tang L, Luo Y, et al. Research progress on drugs for diabetes based on insulin receptor/insulin receptor substrate[J]. Biochem Pharmacol, 2023, 217: 115830.

[25] Croll T I, Smith B J, Margetts M B, et al. Higher-Resolution Structure of the Human Insulin Receptor Ectodomain: Multi-Modal Inclusion of the Insert Domain[J]. Structure, 2016, 24(3): 469-76.

[26] Menting J G, Whittaker J, Margetts M B, et al. How insulin engages its primary binding site on the insulin receptor[J]. Nature, 2013, 493(7431): 241-5.

[27] Ke Z H, Li Y H, Yu A L, et al. Human-relevant doses of bisphenol a induce insulin resistance by downregulating Irs1 expression in skeletal muscle through estrogen receptor-α[J]. Ecotoxicol Environ Saf, 2025, 303: 118791.

[28] Mauvais-Jarvis F, Clegg D J, Hevener A L. The role of estrogens in control of energy balance and glucose homeostasis[J]. Endocr Rev, 2013, 34(3): 309-38.

[29] Muraki K, Okuya S, Tanizawa Y. Estrogen receptor alpha regulates insulin sensitivity through IRS-1 tyrosine phosphorylation in mature 3T3-L1 adipocytes[J]. Endocr J, 2006, 53(6): 841-51.

[30] Gorres B K, Bomhoff G L, Morris J K, et al. In vivo stimulation of oestrogen receptor α increases insulin-stimulated skeletal muscle glucose uptake[J]. J Physiol, 2011, 589(Pt 8): 2041-54.

[31] Mosenzon O, Del Prato S, Schechter M, et al. From glucose lowering agents to disease/diabetes modifying drugs: a "SIMPLE" approach for the treatment of type 2 diabetes[J]. Cardiovasc Diabetol, 2021, 20(1): 92.

[32] Catalano K J, Maddux B A, Szary J, et al. Insulin resistance induced by hyperinsulinemia coincides with a persistent alteration at the insulin receptor tyrosine kinase domain[J]. PLoS One, 2014, 9(9): e108693.

[33] Kahn C R, White M F. The insulin receptor and the molecular mechanism of insulin action[J]. J Clin Invest, 1988, 82(4): 1151-6.

[34] Dongiovanni P, Meroni M, Casati S, et al. Salivary biomarkers: novel noninvasive tools to diagnose chronic inflammation[J]. Int J Oral Sci, 2023, 15(1): 27.

[35] Herrero-Cervera A, Soehnlein O, Kenne E. Neutrophils in chronic inflammatory diseases[J]. Cell Mol Immunol, 2022, 19(2): 177-191.

[36] Margraf A, Lowell C A, Zarbock A. Neutrophils in acute inflammation: current concepts and translational implications[J]. Blood, 2022, 139(14): 2130-2144.

[37] García-Recio E, Costela-Ruiz V J, Melguizo-Rodríguez L, et al. Effects of bisphenol F, bisphenol S, and bisphenol AF on cultured human osteoblasts[J]. Arch Toxicol, 2023, 97(7): 1899-1905.

[38] Schaffert A, Krieg L, Weiner J, et al. Alternatives for the worse: Molecular insights into adverse effects of bisphenol a and substitutes during human adipocyte differentiation[J]. Environ Int, 2021, 156: 106730.

[39] Jaskulak M, Zorena K. Quantifying the metabolic health burden of increased BPA/BPF/BPS endocrine-disrupting chemical exposure: A temporal and cross-country comparative analysis from 2000 to 2024[J]. Sci Total Environ, 2025, 1006: 180897.

[40] Hall M W, Carcillo J A, Cornell T. Immune System Dysfunction Criteria in Critically Ill Children: The PODIUM Consensus Conference[J]. Pediatrics, 2022, 149(1 Suppl 1): S91-s98.

[41] Kim D M, Lee J H, Pan Q, et al. Nutrient-sensing growth hormone secretagogue receptor in macrophage programming and meta-inflammation[J]. Mol Metab, 2024, 79: 101852.

[42] Yao Q, Wang R, Wang H, et al. Total saponins from Panax japonicus alleviate insulin resistance via exosomal miR204/Elovl6-mediated adipocyte-macrophage crosstalk[J]. Phytomedicine, 2025, 142: 156748.

[43] Zhao C, Tang Z, Xie P, et al. Immunotoxic Potential of Bisphenol F Mediated through Lipid Signaling Pathways on Macrophages[J]. Environ Sci Technol, 2019, 53(19): 11420-11428.

[44] Armstrong Suthahar S S, Nettersheim F S, Alimadadi A, et al. Olfr2-positive macrophages originate from monocytes proliferate in situ and present a pro-inflammatory foamy-like phenotype[J]. Cardiovasc Res, 2024, 120(13): 1577-1589.

[45] Iuliano S, Mirabelli M, Giuliano S, et al. Insulin resistance and metabolic dysfunction in thyroid nodules and differentiated thyroid cancer[J]. Curr Opin Oncol, 2026, 38(1): 1-10.

[46] Asker M E, Ali S I, Mohamed S H, et al. The efficacy of bone marrow-derived mesenchymal stem cells and/or erythropoietin in ameliorating kidney damage in gamma irradiated rats: Role of non-hematopoietic erythropoietin anti-apoptotic signaling[J]. Life Sci, 2021, 275: 119388.

[47] Kurmasheva R T, Houghton P J. IGF-I mediated survival pathways in normal and malignant cells[J]. Biochim Biophys Acta, 2006, 1766(1): 1-22.

[48] Cui F, He X. IGF-1 ameliorates streptozotocin-induced pancreatic β cell dysfunction and apoptosis via activating IRS1/PI3K/Akt/FOXO1 pathway[J]. Inflamm Res, 2022, 71(5-6): 669-680.

[49] Taheri R, Mokhtari Y, Yousefi A M, et al. The PI3K/Akt signaling axis and type 2 diabetes mellitus (T2DM): From mechanistic insights into possible therapeutic targets[J]. Cell Biol Int, 2024, 48(8): 1049-1068.

[50] Thimmappa P Y, Vasishta S, Ganesh K, et al. Neutrophil (dys)function due to altered immuno-metabolic axis in type 2 diabetes: implications in combating infections[J]. Hum Cell, 2023, 36(4): 1265-1282.

Supplementary Files

This is a list of supplementary files associated with this preprint. Click to download.

- SupplementaryInformation.docx